Invited Paper

Spatio-Temporal Directional Analysis of 4D Echocardiography

Elsa Angelini [a], Andrew Laine [*a], Shin Takuma [b], Shunichi Homma [b]

[a] Department of Biomedical Engineering, Fu Foundation School of Engineering and Applied Science, Columbia University, New York, NY

[b] Department of Medicine, Echocardiography Laboratories, College of Physicians and Surgeons, Columbia-Presbyterian Medical Center, Columbia University, New York, NY

ABSTRACT

Speckle noise corrupts ultrasonic data by introducing sharp changes in an echocardiographic image intensity profile, while attenuation alters the intensity of equally significant cardiac structures. These properties introduce inhomegenity in the spatial domain and suggest that measures based on phase information rather than intensity are more appropriate for denoising and cardiac border detection. The present analysis method relies on the expansion of temporal ultrasonic volume data on complex exponential wavelet-like basis functions called Brushlets. These basis functions decompose a signal into distinct patterns of oriented textures. Projected coefficients are associated with distinct "brush strokes" of a particular size and orientation. Four-dimensional overcomplete brushlet analysis is applied to temporal echocardiographic volumes. We show that adding the time dimension in the analysis dramatically improves the quality and robustness of the method without adding complexity in the design of a segmentation tool. We have investigated mathematical and empirical methods for identifying the most "efficient" brush stroke sizes and orientations for decomposition and reconstruction on both phantom and clinical data. In order to determine the 'best tiling' or equivalently, the 'best brushlet basis', we use an entropy-based information cost metric function. Quantitative validation and clinical applications of this new spatio-temporal analysis tool are reported for balloon phantoms and clinical data sets.

Keywords: brushlet, spatio-temporal, 3D ultrasound, speckle noise, echocardiography, best basis

1. INTRODUCTION

The recent introduction of real-time true four-dimensional (3D plus time) ultrasound (3DRT) represents an inexpensive, rapid and clinically applicable tool for accurate cardiac function evaluation [1]. Since no interpolation between slices or tomographic reconstruction is required, segmentation is left as the only barrier to automated quantification of physiological parameters such as left ventricular (LV) ejection fraction and wall thickness. Because of hardware limitations, the spatial resolution of volumetric data acquired by this new technology is low (compare to standard 2D echo images) and speckle noise level is quite high. Speckle noise corrupts ultrasonic data by introducing sharp changes in an image intensity profile, while attenuation alters the intensity of equally significant cardiac structures. These properties introduce inhomegenity in the spatial domain and suggest that measures based on phase information rather than intensity are more appropriate for denoising and cardiac border detection [2]. This motivates the development of a new framework to recover information in a domain where speckle noise is decorrelated and an isolated signal may verify known properties.

Brushlet functions are based on a windowed Fourier transform of the Fourier transform of an image with good localization in time and frequency. Windowed Fourier basis of the Fourier plane provide a space-frequency analysis with a better angular resolution than wavelet packets [3]. These basis functions were first introduced by Meyer and Coifman [4] for image compression. They decompose a signal into distinct patterns of oriented textures. Projected coefficients are associated with distinct "brush strokes" of a particular size and orientation. Since brushlet decomposition depends on a signal's spatial frequency content, it is invariant to intensity and contrast range. Four-dimensional overcomplete brushlet analysis is applied to temporal echocardiographic volumes. We show that adding the time dimension in the analysis dramatically improves the quality and robustness of the method without adding design complexity. The underlying hypothesis is that there is a strong coherence in time during diastole and systole phases of the cardiac cycle in the low frequency volumes only and that speckle noise can be reduced dramatically by including the time dimension in an orientation sensitive space-frequency analysis of time-volume data.

Correspondence: Email: laine@columbia.edu

Wavelet Applications in Signal and Image Processing VIII, Akram Aldroubi, Andrew F. Laine, Michael A. Unser, Editors, Proceedings of SPIE Vol. 4119 (2000) © 2000 SPIE · 0277-786X/00/$15.00

As tiling in the Fourier domain determines entirely the structure and utility of the transform, it can be viewed as a hyper-dimension of the analysis. Arbitrary flexibility in partitioning the transform domain allows us to accommodate and precisely match the sampling rates of each acquired dimension (sample spacing in *x, y, z* and *time*). This tiling is a critical parameter of the analysis. In Section 2, we describe two mathematical and empirical methods for identifying the most "efficient" brush stroke sizes and orientations for decomposition and reconstruction on phantoms and clinical data. In order to determine the 'best tiling' or equivalently, the 'best brushlet basis', we used an entropy-based information cost metric function as defined in [5]. Applying a thresholding operator on the diagonal brushlet provided a risk of estimation close to the ideal oracle risk [6]. In Section 3, quantitative results are provided for volumetric phantoms and clinical echocardiographic data sets.

For the rest of the paper, we model the echocardiographic signal $\vec{f}[n]$ contaminated with speckle noise $\vec{W}[n]$ as: $\vec{X}[n] = \vec{f}[n] + \vec{W}[n]$. The signal $\vec{f}$ is estimated by $\tilde{\vec{f}}$ after projecting the noisy data $\vec{X}$ on the brushlet basis $\mathrm{B} = \{\vec{b}_m\}_{m=0,\ldots,N-1}$ and applying a hard thresholding operator ρ_T (at level *T*) on the analysis coefficients $X_{\mathrm{B}}[m] = \langle \vec{X}, \vec{b}_m \rangle$:

$$\tilde{\vec{f}} = \sum_{m=0}^{N-1} \rho_T \left(X_{\mathrm{B}}[m] \right) \vec{b}_m .$$

2. METHOD

Four-dimensional brushlet analysis is applied to temporal phantom and clinical echocardiographic volumes. The analysis is developed in an overcomplete framework to avoid aliasing effects introduced by critical sampling and provide a shift invariant multiscale representation. Adding the time dimension in the analysis can dramatically improve quality and robustness. The underlying hypothesis is that there is a strong coherence in time during diastole and systole for low frequency volume components. In this case, speckle noise can be reduced and anatomical features enhanced by including the time dimension in an orientation sensitive space-frequency analysis.

2. 1. Brushlet Analysis

F. Meyer and R. Coifman first introduced the brushlet functions for compression of highly texturized images [4].

By dividing the real axis into subintervals $[a_n , a_{n+1}]$ of length l_n, we can define a set of brushlet functions $u_{n,j}$ on these sub- intervals as:

$$u_{j,n}(x) = b_n(x - c_n) e_{j,n}(x) + v(x - a_n) e_{j,n}(2a_n - x) - v(x - a_{n+1}) e_{j,n}(2a_{n+1} - x) , \qquad (1)$$

with $c_n = \frac{(a_{n+1} - a_n)}{2}$. The index j $(j \in \mathbb{Z})$ determines the frequency of the complex value exponential $e_{j,n}$ defined as:

$$e_{j,n}(x) = \frac{1}{\sqrt{l_n}} e^{-2i\pi j \frac{(x - a_n)}{l_n}} . \qquad (2)$$

The two window funtions b_n and *v* are derived from the ramp function *r* characterized by the two following properties:

$$r(t) = \begin{cases} 0 & if \quad t \le -1 \\ 1 & if \quad t \ge 1 \end{cases}$$

and (3)

$$r^2(t) + r^2(-t) = 1 , \ \forall t \in \mathbb{R} \quad .$$

Detailed description of the construction of brushlet functions and their numerical implementation can be found in [4].

We can project $\hat{f}$ on a brushlet basis, $\hat{f} = \sum_n \sum_j \hat{f}_{n,j} u_{n,j}$ where $\hat{f}_{n,j}$ are the brushlet coefficients. By applying an inverse Fourier transform, we can compute a decomposition of f, $f = \sum_n \sum_j \hat{f}_{n,j} w_{n,j}$, on the orthonormal basis $w_{n,j}$, inverse Fourier transform of $u_{n,j}$, and defined as:

$$w_{n,j}(x) = \sqrt{l_n} e^{2i\pi a_n x} e^{i\pi l_n x} \left\{ (-1)^j \hat{b}_\sigma (l_n x - j) - 2i \sin(\pi l_n x) \hat{v}_\sigma (l_n x + j) \right\} \quad (4)$$

The parameter ε controls the degree of localization of the brushlet function and its inverse Fourier transform in time and frequency. The smaller the value of ε, the better the localization in frequency (smaller second peak shown in Figure 1.b) but the localization in time becomes less (spread of the central peak). This tradeoff in time-frequency resolution is analogous to the Heisenberg uncertainty principle that controls wavelet packet resolution. We can observe in Equation (4) the wavelet-like structure of the $w_{n,j}$ functions with scaling factor l_n and translation factor j. The major difference between brushlet basis and wavelet packets is the arbitrary tiling of the time-frequency plane and the perfect localization of a single frequency for one coefficient. An example of an analysis brushlet function and its associated reconstruction function is provided in Figure 1 below.

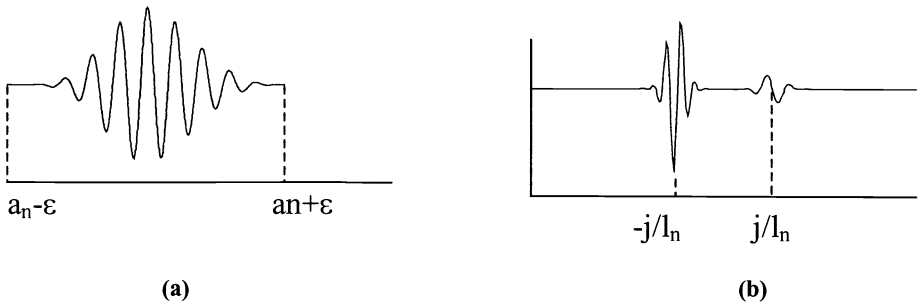

Figure 1: (a) Analysis brushlet function $u_{n,j}$, defined on an interval of length ln. (b) Associated synthesis function $w_{n,j}$, with two peaks localized at -j/ln and j/ln.

In order to control the oscillations of a brushlet $w_{n,j}$ it is desirable to have a positive Fourier transform of the windowing function b. However, this condition is not compatible with the original construction of the $u_{n,j}$ functions as in Equation (1). Meyer and Coifman thus introduced two biorthogonal windowed Fourier bases: synthesis function $w_{n,j}$ and dual analysis functions $\tilde{u}_{n,j}$. In order to have $\hat{b}$, the Fourier transform of b, positive, they relaxed conditions on the ramp function defined in Equation (2) and defined a new ramp function with the following properties:

$$\begin{cases} r(t) = 0 \quad if \quad t \le 1 \\ \text{and} \\ r^2(t) + r^2(-t) > 0, \forall t \in \mathbb{R} \end{cases} \quad (5)$$

Imposing $\hat{b} \ge 0$ implies for the second derivative that $b''(0) < 0$ so that the bell function b cannot be flat around 0. This condition imposes that $\varepsilon = l_n / 2$. In our implementation we followed the suggestion of Coifman and Meyer and defined b as a cubic spline so that $\hat{b}$ was equal to: $\hat{b}(\xi) = \left(\frac{\sin(\pi\xi)}{\pi\xi} \right)^4 \ge 0$. The analysis functions $\tilde{u}_{n,j}$, dual to the reconstruction functions $w_{n,j}$, are then defined as in Equation (1) by replacing b and v by $\tilde{b}$ and $\tilde{v}$ defined with the new ramp function $\tilde{r}(t) = \frac{r(t)}{r^2(t) + r^2(-t)}$.

2. 2. Multidimensional Implementation

The implementation of the brushlet analysis in higher dimensions is straightforward. The tensor product structure of the basis allows a direct extrapolation of the 1D case to n-D. In terms of implementation, we used the folding operator introduced by Wickerhauser [7] to project the signal on the complex exponential brushlet basis functions. For a given volume data, (1) its n-D Fourier transform is first computed, (2) n-D tiling is applied, (3) individual sub-volumes are folded along each dimension, (4) and finally folded sub-volumes are expanded onto the complex exponential functions via a second n-D Fourier Transform.

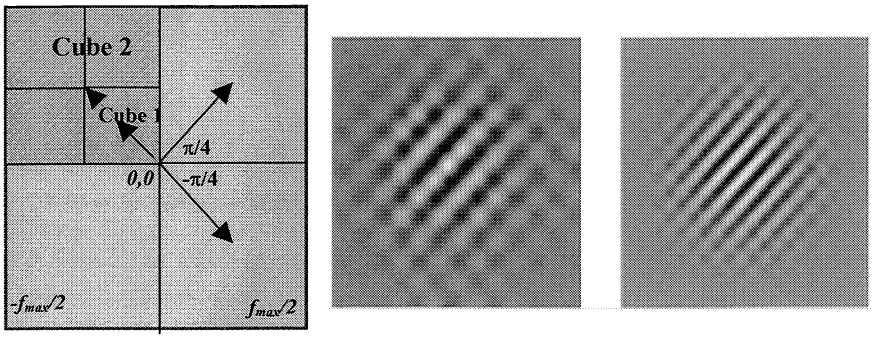

Figure 2: Illustration in 2D of the influence of the tiling of the Fourier domain on the resolution and orientation of a brushstrokes. (a) Tiling of the Fourier domain. (b) Real-Part of coefficient for Cube 1. (c) Real-Part of coefficient for Cube 2.

In n-D, each sub-volume is associated with a brushstroke whose orientation is determined by the position of the center of the sub-volume in the Fourier domain and whose resolution is determined by the size of the sub-volume. An example in 2D is provided in Figure 2 for two brushstrokes corresponding to two quadrants with same orientation but different resolution.

2. 3. Overcomplete analysis

The size of the sub-volumes created with a tiling of the Fourier domain determines the size of the coefficient set associated with each characteristic brushstroke. The diminution of dimension between the spatial domain and the transform domain is analogous to a two-fold downsampling observed in dyadic wavelet analysis between consecutive scales. In order to overcome the problems of downsampling, we developed an overcomplete framework, best suited for image analysis and denoising/enhancement, as it avoids aliasing effects introduced by critically sampled representations [8] and yields a shift invariant representation.

In the case of brushlets, the aliasing effect arises from the selection of overlapping subintervals on the Fourier plane that are expanded into a local Fourier basis. To avoid this and increase the number of coefficients within the same subinterval size, we project onto an extended Fourier basis. This increases the matrix size in the projection domain without changing the original signal. The overcomplete projection is efficiently implemented by simply padding the folded signal with zeros before computing the final FFT. Since padding a signal will increase the resolution of the FT, overcomplete projections increase the number of coefficients for the same frequency interval and therefore improves resolution in the transform (coefficient) domain. An example of overcomplete vs. decimated brushlet decomposition is presented in Figure 3.

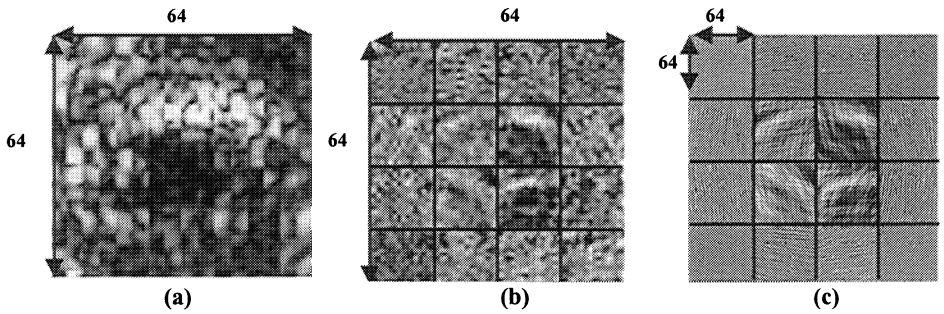

Figure 3: Example of decimated and overcomplete brushlet analysis for a single plane of 3D ultrasound data. (a) Original cardiac ultrasound slice. (b, c), Real-Part of coefficients for a 16-quadrant tiling of the Fourier plane in the non-overcomplete case (b), and overcomplete case (c). Actual dimension of the original image and the sub-quadrants coefficients are indicated.

2. 4. Estimation of noise variance

Envelope-detected ultrasound signals with fully developed speckle can be modeled with a Rayleigh distribution [9, 10]. In this framework, the following signal-dependent noise model can be used to represent ultrasound signals:

$$X = f + \sqrt{f}\,n, \tag{6}$$

where X is the observed signal, f is the true signal and n is the zero-mean noise component, independent of the true signal s. In a uniform area where the true signal is constant $(f = F)$ we have:

$$\sigma_X^2 = F.\sigma_n^2, \tag{7}$$

where σ_X^2 is the variance of the observed signal X and σ_n^2 the variance of the noise n. This property has been used for various adaptive-filtering approaches for denoising of B-scans ultrasounds [10-12]. In order to estimate the variance we define local mean and variance for a window of size $[M\ N]$:

$$\begin{aligned} \mu_{i,j} &= \frac{1}{M\,N}\sum_{m=-M/2}^{M/2}\sum_{n=-N/2}^{N/2} X_{i-m,j-n} \\ \sigma_{i,j}^2 &= \frac{1}{M\,N}\sum_{m=-M/2}^{M/2}\sum_{n=-N/2}^{N/2}\left(X_{i-m,j-n} - \mu_{i,j}\right)^2 \end{aligned} \tag{8}$$

where $X_{i,j}$ is the gray value of pixel *(i, j)*, $\mu_{i,j}$ the mean value and $\sigma_{i,j}^2$ the variance of the observed signal at the same location. We call α the ratio of the local variance over the local mean:

$$\alpha(i,j) = \sigma_{i,j}^2 \big/ \mu_{i,j}\ , \tag{9}$$

In uniform areas where Equation (7) is verified, we observe:

$$\alpha(i,j) = \mu_{i,j}.\sigma_{n\,i,j}^2 \big/ \mu_{i,j} = \sigma_{n\,i,j}^2 . \tag{10}$$

Hence, $\alpha(i,j)$ provides a good approximation of the local variance of the speckle noise in homogeneous areas where the true signal is constant and Equation (7) is almost verified. Hao et al [11] used this approximation to define median filters weights as a function of the local variance of the noise in ultrasound images.

In our application, three homogeneous areas are defined in the ultrasound volume corresponding to the myocardium muscle wall, the inside cavity and the outside space. In three dimensions, we used a window of size $[6\times6\times2]$ to estimate the noise variance volume Λ with results displayed in Figure 4.

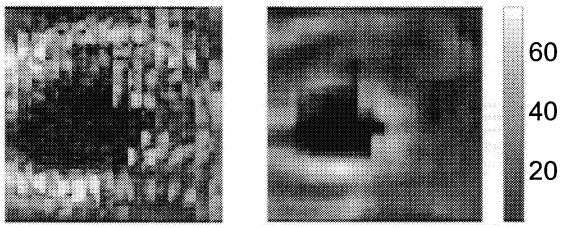

(a) **(b)**

Figure 4: Estimation of speckle noise variance in echo volume. (a) Original slice extracted from temporal volumetric data set. (b) Corresponding speckle noise variance slice, extracted from variance volume.

2. 5. Hard Thresholding

After analyzing the signal on the brushlet basis functions, we zero-out the higher frequency coefficients and apply a hard thresholding to the lower frequency coefficients prior to reconstruction. Hard thresholding of the coefficients aims at eliminating the influence of noise components, while preserving signal components, hopefully concentrated in few coefficients of large magnitude. The risk of applying a hard thresholding operator ρ_T (at level T) on the analysis coefficients is:

$$r(f) = \sum_{n=0}^{N-1} E\left\{\left|f_B[n] - \rho_T\left(X_B[n]\right)\right|^2\right\}\ , \tag{11}$$

with $f_B[n] = \langle \vec{f}, \vec{b}_n \rangle$ and $X_B[n] = \langle \vec{X}, \vec{b}_n \rangle$.

The non-linear projector that minimizes this risk is the hard thresholding operator that keeps coefficients $X_B[n]$ only if $|f_B[n]| > \sigma_W$, with σ_W the variance of the noise $\vec{W}$ [13]. In this case the risk of estimation is minimal: $r_{oracle} = \sum_{n=0}^{N-1} \min\left(\left|f_B[n]\right|^2, \sigma_W^2\right)$. It is called and oracle risk since we do not know $|f_B[n]|$. By applying a similar hard thresholding to the coefficients $X_B[n]$ where the condition $|f_B[n]| > \sigma_W$ is replaced by $|X_B[n]| > \sigma_W$, using the noise variance estimated from the data, we hope to remain close to the ideal oracle risk.

2. 6. Best Basis framework

The tiling of the Fourier domain determines entirely the structure of the transform domain and can be viewed as a hyper-dimension of the 4D analysis. The choice of the tiling determines at which frequencies the original signal is analyzed and at which resolution it is expanded. The flexibility in partitioning the transform domain allows us to accommodate and precisely match the different sampling rates of each acquired dimension (sample spacing in *x, y, z* and *time*). This tiling is a critical parameter of the analysis as it allows us to systematically adjust specific brushlet coefficients for noise reduction and selectively reconstruct salient features of interest. We have investigated empirical and mathematical methods for identifying the most "efficient" brush stroke sizes and orientations for decomposition and reconstruction on phantoms and clinical data:

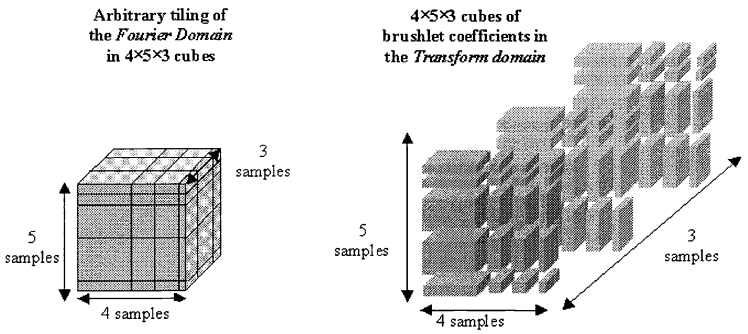

Figure 5: (a) 3D tiling of the Fourier domain with arbitrary sampling along each direction. (b) Corresponding structure of brushlet coefficients in the transform domain.

(a) Empirical testing was carried out for regular tiling with 2, 4 and 8 sub-intervals along each dimension
(b) Computational method to select the best tiling followed the 'best basis' framework of Wickerhauser [5]. The information cost metric is the entropy functional [14] defined as:

$$E(f, \mathcal{B}) = \sum_{n=0}^{N-1} \min\left(X_B^{\mathcal{B}}[n]^2, \sigma_W^2\right). \quad (12)$$

The best basis $\boldsymbol{B}$ for estimating the signal f minimizes the risk of estimation via hard thresholding with threshold value set to the estimated variance of the noise σ_W^2:

$$E(f, \boldsymbol{B}) = \min_{\mathcal{B}}\left(\sum_{n=0}^{N-1} \min\left(X_B^{\mathcal{B}}[n]^2, \sigma_W^2\right)\right) \quad (13)$$

3. RESULTS

3. 1. Optimal concentration of signal component in 4D compare to 3D analysis

To quantitatively evaluate the performance of our dynamic 4D analysis in decorrelating noise components in lower frequencies, we first tested it on a mathematical phantom. The phantom consisted of an ovoid volume growing in time that schematically mimicked aspects of the left ventricle with an inner gray cavity surrounded by a thick white wall on a black background. The size of a single volume was 64×64×64 and there were 16 volumes growing in time. The volume increased by 70% over 16 time frames, similar to the average ejection fraction in normal patients.

We carried out a 3D and 4D brushlet analysis with four subintervals in each direction on the original 4D volume and on volumes with (1) additive white noise, (2) and multiplicative speckle noise. Volumes were reconstructed with only the lower frequency components.

- In the case of additive white noise (mean 0 and standard deviation 1), the SNR of the noisy volume was -5.7dB. We measured a SNR of -4.3dB (a 25% improvement) with 3D brushlet analysis and -3.6dB (a 37% improvement) with 4D brushlet analysis.
- In the case of multiplicative speckle noise (mean 0 and standard deviation 1), the SNR of the noisy volume was -19.7dB. In Figure 6 the same slice is displayed in the transform domain after a 3D analysis on a single time frame or a 4D analysis with the entire set of 16 frames. Visually, the 4D analysis performed slightly better at denoising the data. Quantitatively, we measured a SNR of -13.4dB (a 32% improvement) with 3D brushlet analysis and -13.0dB (a 34% improvement) with 4D brushlet analysis.

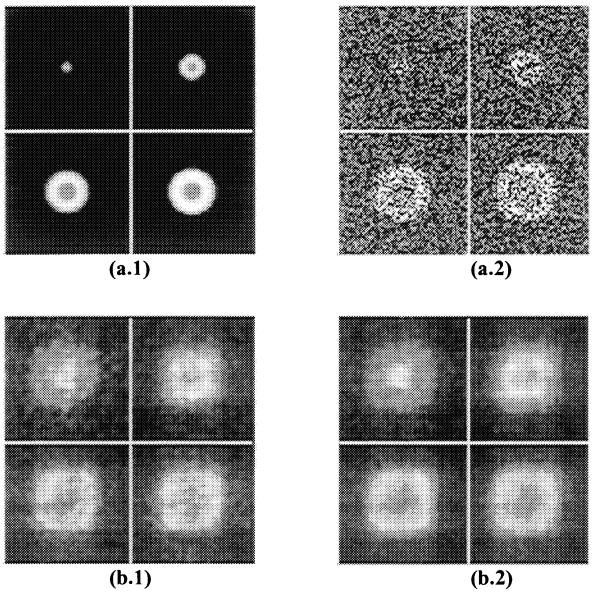

Figure 6: Comparison of speckle-denoising performance in the coefficient domain for 3D and 4D brushlet analysis. (a.1) Four slices of original volume in one time frame, (a.2) slices after addition of multiplicative speckle noise (SNR=-19.7dB), (b.1) corresponding slices in coefficient domain for 3D brushlet analysis (SNR=-13.4 dB), (b.2) corresponding slices in coefficient domain for 4D analysis (SNR=-13.0dB).

3. 2. Reconstruction of wall defect with 4D analysis

Performing multidimensional analysis on cardiac clinical data takes full advantage of the continuity of spatial and temporal frequency content of multidimensional signals. The high level of speckle noise in ultrasound clinical data sets recorded with the 3D real-time transducer, the non-uniform absorption coefficients of cardiac tissues and the motion of the heart contribute to the addition of artifacts that can either add echo-like signals inside the cavity or suppress echo signals from the myocardium wall. These artifacts complicate the segmentation task by introducing artificial edges inside the cavity or destroying edges at the epicardium and endocardium borders. Since these artifacts are not persistent in time, including the temporal component in the analysis helps resolve them. To illustrate the aptitude of the brushlet analysis to repair missing contour information, we modified the mathematical phantom used in Section 3.1. The same ovoid phantom was used, but a part of the white wall has been eliminated in the eighth time frame. Both 3D analysis on the time frame with the defect and 4D brushlet analysis applied to the sixteen time frames were computed. For both cases, the sum of the coefficients of lower

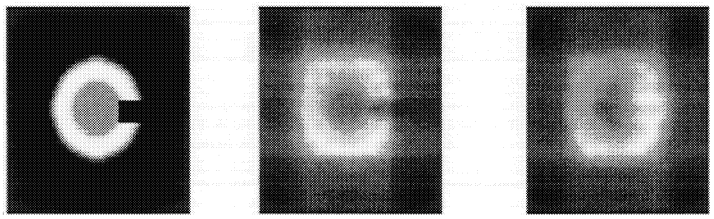

Figure 7: (a) Original slice with defect. Corresponding slice in transform domain for: (b) 3D analysis of single time frame and (c) 4D analysis of 16 time frames.

frequency for the eighth time frame (with the defect) is displayed in Figure 7. We observed remarkable correction in the wall defect with the 4D transform domain (3D + *time*) that could not be obtained with 3D analysis alone.

3. 3. Optimal tiling on clinical data

We carried out brushlet analysis and thresholding prior to reconstruction on a clinical data set with sixteen echocardiographic volumes of size [64 × 64 × 256] in the [$x \times y \times z$] directions. The sixteen frames contain the cardiac chamber volume at different times during one cardiac cycle. To limit computational cost and to reduce the level of noise, the original data set was down-sampled in the z direction by averaging every four consecutive slices, prior to analysis.

3.3.1. Empirical results with regular tiling

Empirical regular tiling was applied for 2, 4 and 8 subintervals in the *x, y and z* directions. Since there were only sixteen time frames, the time dimension t was only divided in 2 or 4 subintervals. Hard thresholding was then applied, using the estimated noise variance of the original volumes, prior to reconstruction. The tiling of the Fourier domain has a critical influence on the quality of the estimation of the echo signal and the resolution of the denoised data. This influence is illustrated in Figure 8 where a single slice of an original volume (*time*=5, after averaging in the z dimension) and corresponding reconstructed slices with different tiling are presented. The slice displays a short-axis cut of the left ventricular cavity (dark center cavity) surrounded by the myocardium muscular wall (white ring).

As predicted in theory, when the number of sub-intervals increases, the frequency resolution of the analysis increases but the spatial resolution of the reconstruction decreases. This phenomenon, which can be observed in the results presented in Figure 8, makes the task of evaluating the performance of the selected tiling in terms of enhancement – denoising difficult. How can we decide that one tiling is better than another one for volume segmentation? One requirement is that no anatomical features should be eliminated from the original data. This means that too fine tilings should not be investigated since the spatial resolution during the reconstruction will be low. On the other hand, large sub-intervals will not be capable of eliminating high frequency speckle-noise components.

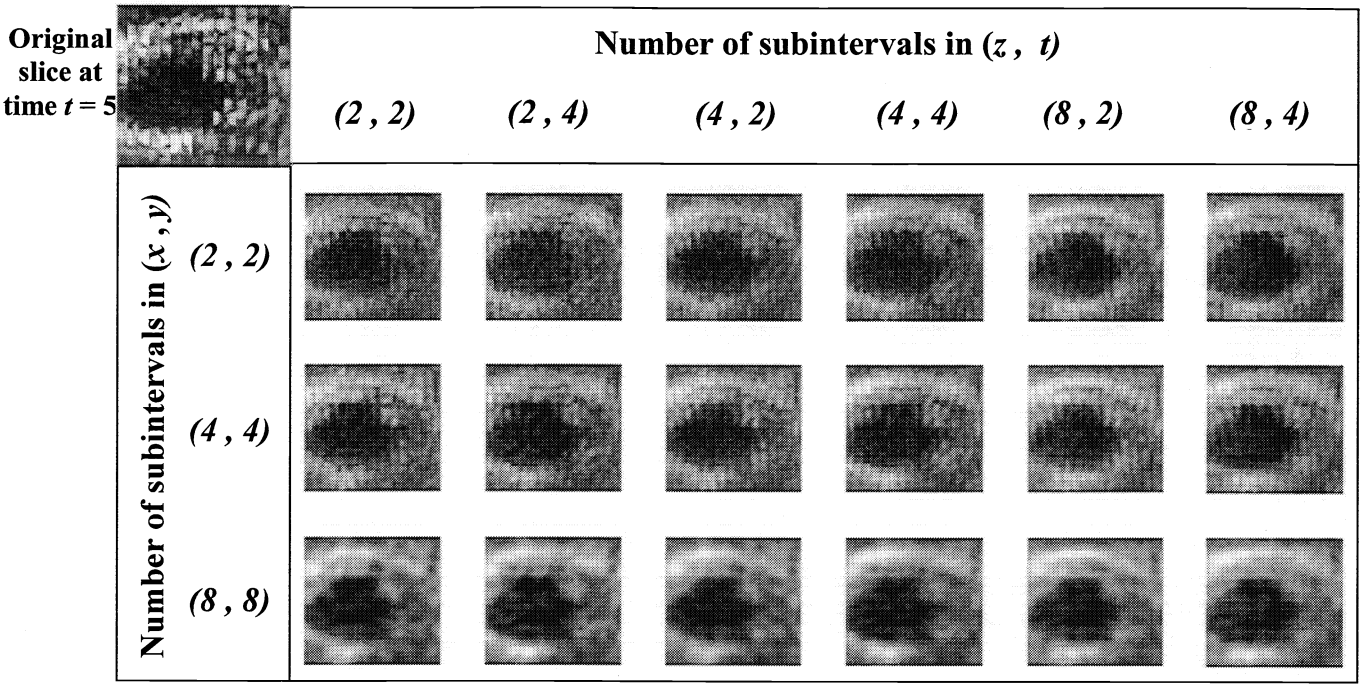

Figure 8: Slice reconstructed after hard thresholding of brushlet coefficients for different tilings of the Fourier domain in 4D.

3.3.2. Optimal tiling with best-basis search

In order to validate our method, we first ran the best basis algorithm with the brushlet basis on a phantom image composed of a white diagonal line with black background. The result of the best basis search with L^3 and L^5 norms is presented in Figure 9. Since the L^1 norm only measures the number of coefficients different from zero, and the L^2 norm is constant, we used L^p norms with $p>2$ to measure the good concentration of the energy of the signal in few coefficients. The result shows that only the diagonal quadrants of the Fourier plan with non zero frequency components are decomposed in fine grids (note that there is a 90 degree shift between the location of the quadrant in the Fourier plan and the brushlet orientation).

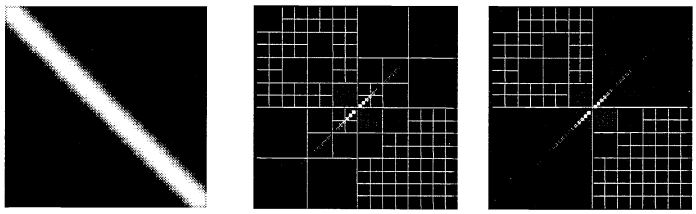

(a) (b) (c)

Figure 9: (a) Original image with diagonal line. (b) Fourier Transform of the image overlaid with optimal tiling for L^3 norm. (c) Fourier Transform of the image overlaid with optimal tiling for L^5 norm.

We then applied the algorithm of best-basis search in 3D on one of the clinical volume (*time*=5) used in Section 3.3.1. The optimal tiling of the Fourier volume came out to be the regular tiling with 4 subintervals in each dimension except in the higher frequency quadrant where only a 2×2×2 tiling is applied. This appears to be a good compromise between spatial and frequency resolutions with: (a) no selection of specific directional components in lower frequency, and (b) a coarse decomposition of higher frequency terms containing principally speckle noise components with no coherence. The spatial symmetry of the myocardium cavity can also explain such result that preserves the isotropy of the spatial information.

4. DISCUSSION

By applying 4D brushlet analysis to clinical ultrasound volumes we were able to decorrelate speckle noise from echo signals and enhance myocardial anatomical features.

The performance of brushlet analysis to decorrelate signal from multiplicative speckle noise components was demonstrated on a mathematical phantom in 3D and 4D and on a clinical data set. The example on the phantom showed the superiority of 4D denoising over 3D denoising for 4D data sets. It also showed that including temporal information in the analysis enabled correction of artifacts that are not persistent in time.

The main power of a brushlet expansion is its flexibility in decomposing *n*-D signals and its ability to accommodate and precisely match non-uniform sampling rates of each dimension typically obtained during 3DRT acquisition (independent sample spacing in *x, y, z* and *time*). The multidimensionality of the brushlet analysis and its flexibility to accommodate different sampling rates in different directions represent a potential for new analysis tools tailored to underlying sampling rates. We observed that tiling in the directions of lowest sampling has the most effect on the image quality of the reconstruction in terms of denoising and enhancement.

We applied denoising to 3DRT volumes by analyzing the data sets in 4D and applying hard thresholding on the coefficients prior to reconstruction. The thresholding of the coefficients was based in the estimated variance of the noise. This thresholding tried to minimize the estimation error risk [6]. The model used for speckle noise, initially proposed by Hao [11] appeared to be appropriate for the denoising of the coefficients via hard thresholding.

The tiling of the Fourier domain determined the orientation and the resolution of the brush strokes on which the signal was projected. In other words, the tiling selects the textural patterns used for the analysis of the original signal. From this point of view, tiling can be considered as an extra dimension of the analysis. The optimization of analysis parameters can be derived from mathematical modeling of the ultrasound data, based on the physics of the transducer and properties of the volumetric data. The best basis approach [5] applied to the brushlet for ultrasound volumes selected a regular tiling in each dimension, with coarser tiling of higher frequency components, providing a reasonable compromise between spatial and frequency resolution.

5. CONCLUSION

This study showed that we could characterize and isolate features of interest in 4D echocardiographic volumes by selection of specific brushlet coefficients. The spatio-temporal analysis method developed for this task used directional multiscale brushlet functions. Brushlet analysis identifies efficient tiling of the Fourier domain, along each dimension of a signal, within sets of redundant articulated (orientation rich) bases that can separate signal and noise components. The mathematical innovation lies in the inclusion of the time dimension with arbitrary tiling of the 4D Fourier domain. This multidimensionality and the flexibility of the analysis functions to accommodate different sampling rates along each direction represents a potential for new analysis tools tailored to true sampling rates. The optimization of analysis parameters can be derived from both mathematical modeling of the ultrasound data, based on the physics of the transducer and properties of the volumetric data. Accurate modeling of the physics of acquisition of ultrasound data in the construction of the expansion resulted in efficient representations for dynamic denoising and analysis of cardiac features.

ACKNOWLEDGEMENTS

This project was supported in part by the Whitaker Foundation.

REFERENCES

[1] S. Takuma, T. Ota, T. Muro, I. Oropesa, R. Sciacca, L. Mendoza, M. R. D. Tullio, D. K. Blood, J. Yoshikawa, and S. Homma, "Assessment of left ventricular function by real-time 3D echocardiography compared with conventional noninvasive methods," 10th Annual Scientific Sessions American Society of Echocardiography, Washington DC, 1999

[2] E. Angelini, A. Laine, S. Takuma, and S. Homma, "Directional representations of 4D echocardiography for temporal quantification of LV volumes," Medical Imaging and Computer-Assisted Intervention - MICCAI'99, Cambridge, England, 1999, pp. 430-440.

[3] M. V. Wickerhauser, "Smooth localized orthonormal bases," *Comptes Rendus de l'Academie des Sciences, Paris I*, pp. 423-427, 1993.

[4] F. Meyer and R. R. Coifman, "Brushlets: A tool for directional image analysis and image compression," *Applied and computational harmonic analysis*, vol. 4, pp. 147-187, 1997.

[5] M. V. Wickerhauser, "The Best Basis Algorithm," in *Adapted Wavelet Analysis from Theory to Software*, W. A. K. Peter, Ed., 1993, pp. 273-298.

[6] S. Mallat, *A Wavelet Tour of Signal Processing*. San Diego, CA: Academic Press, 1998.

[7] P. Ausher, G. Weiss, and M. V. Wickerhauser, "Local sine and cosine bases of Coifman and Meyer and the construction of smooth wavelets," in *Wavelets- A tutorial in Theory and Applications*, vol. 2, *Wavelet Analysis and its Applications*, C. K. Chui, Ed. San Diego: Academic Press, 1992, pp. 237-256.

[8] X. Zong, A. F. Laine, and E. A. Geiser, "Speckle reduction and contrast enhancement of echocardiograms via multiscale nonlinear processing," *IEEE Transactions on Medical Imaging*, vol. 17, pp. 532-540, 1998.

[9] V. Dutt, *Statistical Analysis of Ultrasound Echo Envelope*. Ph.D Thesis from Ultrasound Research Laboratory, Mayo Foundation, Rochester, MN, 1995 .

[10] T. Loupas, W. N. Mcdicken, and P. L. Allan, "An adaptive weighted median filtering for speckle suppression in medical ultrasonic images," *IEEE Transaction on Circuits and Systems*, vol. 36, pp. 129-135, 1989.

[11] X. Hao and S. Gao, "A novel multiscale nonlinear thresholding method for ultrasonic speckle suppressing," *IEEE Transaction on Medical Imaging*, vol. 18, pp. 787-794, 1999.

[12] M. Karaman, A. Kutay, and G. Bodgazi, "An adaptive speckle filter for medical ultrasonic imaging," *IEEE Transaction on medical imaging*, vol. 14, pp. 283-293, 1995.

[13] D. L. Donoho and I. M. Johnstone, "Ideal spatial adaptation by wavelet shrinkage," Statistics Department, Stanford University, Technical Report 1992.

[14] D. L. Donoho and I. M. Johnstone, "Ideal denoising in an orthonormal basis chosen from a library of bases," Statistics Department, Stanford University, Technical Report 1994.